

Research Article

Cite this article: Sağlam Ü, Tekin A (2020). Resonance-filtering combo system for continuous wireless charging range coverage. *Wireless Power Transfer* 7, 116–125. <https://doi.org/10.1017/wpt.2020.12>

Received: 7 January 2020
Revised: 22 August 2020
Accepted: 8 September 2020
First published online: 19 October 2020


Key words:

Dual-frequency wireless charger; uniform wireless charging; wireless power transfer

Author for correspondence:

Ahmet Tekin, Özyeğin University,
Analog & RF Research Labs, Istanbul, Turkey.
E-mail: ahmet.tekin@ozyegin.edu.tr

Resonance-filtering combo system for continuous wireless charging range coverage

Üstün Sağlam^{1,2} and Ahmet Tekin¹ 

¹Özyeğin University, Analog & RF Research Labs, Istanbul, Turkey and ²Vestel Electronics, Power Electronics Research Labs, Manisa, Turkey

Abstract

Distribution of wireless power charging field uniformly on a large area pad is critical for power receivers, particularly for wearable devices, wherein small form factor coils are involved. Since the receiver coil size is quite limited in these types of applications, the device is very sensitive to the amount of field it could retain and hence, it needs special placement or snapping mechanism to fix it at an optimum location for reliable wireless charging. In order to overcome this limitation for the end-user, a dual-mode multi-coil power transceiver system is proposed; utilizing resonance filtering to increase the amount of total power delivered with the rather uniform spatial distribution. Two concentric coils; center one driven by 6.78-MHz high-frequency driver (A4WP) and the outer larger one with a 200-KHz low-frequency driver (Q_i) with resonant blocker could transfer up to 50 mW standards compliant flat power to a 13-mm radius 30-turns wearable receiver coil everywhere across an 8-cm radius charging pad area without any alignment requirement or snapping. Two different feedback topologies corresponding to each of the H-Bridge power drivers were also presented as an automatic series resonance coil drive frequency lock mechanism, extracting peak powers for each system individually from a standard 5 V-1A USB wall charger.

Introduction

The proliferation of wireless power transfer systems is quite noticeable these days in many realms of our lives. There are multiple research problems that need to be addressed and also many system and circuit level features that must still be improved in wireless power transfer field, in order to attain wider market penetration. The efficiency of the system [1–3], distance optimization between the transmitter and receiver coils [1, 4], and as the most related this work; uniform magnetic field distribution [5–7], on a charging pad are examples of currently on-demand research activities. Moreover, there are two competing wireless power transfer standards on the scene; Q_i and A4WP that the designers should carefully consider while designing the corresponding electronics around their particular system. Performance of the design may vary for each wireless power transfer standard. Both Q_i and A4WP standards have some advantages and disadvantages with respect to each other.

Q_i standard was proposed by Wireless Power Consortium (WPC) and has a wide operating frequency range of 87–205 KHz [8]. Q_i standard compliant systems have high efficiency by close-in inductive coupling [9]. Coupling coefficient for these closely coupled coil systems must be close to 1, which is the maximum number for an ideal transfer case [10]. Thus, the distance between the transmitter and receiver has to be just a few millimeters [9]. T_X coil of a typical Q_i system usually has a much higher inductance value than competing A4WP's high-frequency T_X coil. Hence the coil size and number of turns are usually much larger than the other. The large coil of Q_i sub-system, hence, has non-uniform field distribution decaying fast towards the center. One remedy to this drawback would be to introduce more number of turns close to the center for enhanced coverage, but, this comes with a cost of the weaker field close to the outer turns. Hence, a more attractive solution is needed to cover large charging areas.

A4WP standard compliant systems, on the other hand, operate at 6.78 MHz Industrial, Scientific, and Medica (ISM) band and the specified deviation tolerances of this center frequency are just ± 15 kHz which is much narrower than Q_i allowed frequency limits [11]. Tight frequency limits for A4WP make the frequency control difficult because of environment-dependent factors in the system [11]. Small form factor coils can be designed with relatively high-quality factor [10] and the ripple performance of the output voltage of receiver is better due to high frequencies. Despite these advantages of high-frequency operation, parasitic affects limit the efficiency due to additional switching losses associated [12]. Magnetic fields generated by T_X coil are strong in the central areas while it degrades at the outer boundaries moving away from the charging coil in this high-frequency system.

In order to increase the efficiency of a wireless charging system, magnetic shielding is vital and widely used in most wireless charging systems. They can be used under the transmitter coil, above the receiver coil or both together. Ferrite sheet shows low impedance to the magnetic field passing through it [13]. Loss in magnetic field intensity decreases and coupling between transmitter and receiver coils increases and hence the overall transfer efficiency as elaborated in [14, 15]. The presence of the ferrite sheet under the transmitter coil increases the inductance of the transmitter coil, too. Magnetic shielding enhances the coupling and as a result, reliable power transfer distance between transmitter and receiver could increase. Effectiveness of the shielding depends on the overall permeability and thickness of the magnetic sheet.

Designing both Q_i and $A4WP$ compliant combo system is an active research topic to exploit the benefits of both. Each power receiver device belonging to a particular wireless charging standard needs a transmitter which should resonate along with the same standard specifications. There is a significant amount of effort underway to combine different standards with full compatibility on the receiver side or even on the transmitter side. In [16], both 200 kHz and 6.78 MHz supported transmitters and receivers are studied. This system is developed to negotiate negative interactions between the 200-kHz and the 6.78-MHz pieces. This particular system works dual-band. Two 200-kHz and 6.78-MHz supported transmitters transfer the energy to two 200-kHz and 6.78-MHz supported receivers, respectively. This particular system is effectively dual- T_X and dual- R_X topology, whereby it puts multiple constraints in the receiver device, which has to be extremely small for the target wearable applications. In [17–19], trade-offs with respect to different wireless power standards have also been studied. In [12], both low and high-frequency effects were studied just paying attention to the receiver side to improve the reception. In most of the cases, the main motivation in combining dual-mode transmitter coils is to reach a universal charger device that can charge any receiver. The work in this study targets the dual system for rather a different purpose; namely, getting more and uniform power to a small receiver coil across a wide charging pad area. In this case, the special receiver side design is a wideband circuit which has no series or parallel resonant element for the low-band; treating the received combo signal at both the low- and high-frequency band as the full charging resource.

Small wearable device charging targeted in this work is a particularly hard task to implement because of the small form factor receiver coils involved. Suggested wireless charging systems require larger receiver coils to collect the energy of the generated magnetic field. However, the size is quite limited in these types of applications. Hence, the coupling would be weak and efficiency would be low to maintain charging voltage levels larger than even the threshold levels of the rectifier. Research done in the field recently shows that the size, cost, and efficiency are all tightly related and must all be considered carefully in wearable devices [11, 20, 21]. It is particularly hard to drive the small form factor receiver coil since the transmitted power level changes wildly according to the placement of receiver (R_X) coil on a relatively large charging pad. Large transmitter (T_X) coil does not generate equal magnetic field strength across all the regions along this pad. Hence, the coupling factor k and the power delivered to the load changes depending on the location of the small receiver. Uniformity of generated magnetic field, hence, becomes a quite key design consideration not to end up with partially working

design. An additional important design criterion for small form factor receivers is then; the total amount of spatially uniform power that could be delivered. Most of the wireless charger research provided above review addresses this particular issue by either proposing a unique multi-section area optimized coil design or going multi-coil overlapping structures. In both cases, however, the major drawback is the loss associated with the regions corresponding to the superposition of out-of-phase signals. This paper has investigated a rather different approach, namely; superimposing uncorrelated orthogonal signals, one low and one order of magnitude higher frequency.

In this work, a Q_i and $A4WP$ compliant combo power transfer system for small form factor wearable device applications is presented. The combo system has not only helped the total amount of power that could be transferred but also assured spatial charging uniformity across the wide charging pad which resulted in more comfort in user experience. Design trade-offs in relation to concurrent multi-driver co-centric coil design as well as performance enhancement due to the proposed resonant filtering technique were all discussed in detail along with the measurements from the actual design prototypes. In the small central space of a large low-frequency coil, a well-tuned high-frequency coil system can yield a significant boost in the overall power transfer level if the cross-loading losses between the coils were avoided. Extending the transmitter coil of the low-frequency system towards the center for more areal coverage in a single-frequency system could not yield the same level of improvement as an additional separate high-frequency coil resonance transmitter could do in the same small space left. This work implemented just a simple resonance filter to reduce cross-coupling of these co-centric coils and enhance the proposed benefits of a combo system. Moreover, in order to extract the maximum amount of power from each of the driver sub-systems, two separate analog and digital feedback loops were proposed, keeping each of the transmitter systems in their corresponding resonance lock regardless of their mutual interaction and variable load conditions.

The paper is organized as follows: the section “Implementation of combo wireless charger system” goes through the circuit details of the proposed combo system. In the section “Experimental results” the experimental results of a prototype of the proposed technique were presented along with the similar performance results from the experiments with the existing stand-alone individual Q_i and $A4WP$ charging circuits. The section “Conclusion” concludes the paper and the section “Future work” mentions some future work that may improve the particular combo system further.

Implementation of combo wireless charger system

Coil design

In order to get uniform magnetic fields in a wide range on the charging pad, low frequency and high-frequency sub-systems were combined allowing both transmitters operate concurrently. This is done by co-centric placement of the $A4WP$ transmitter coil inside of Q_i transmitter coil, whereby uniform magnetic field density can be obtained. Since the Q_i coil operates at a relatively lower frequency, it can be large and outside; while $A4WP$ coil is placed at the center. $A4WP$ transmitter coil generates strong magnetic fields at the center of the structure and Q_i transmitter generates a strong magnetic field near the outer windings. The magnitude of the magnetic field at a point X distance away from the center of a current-carrying loop with radius R depends

on the amount of current flowing as well as the distance between the wire and the point which is expressed by;

$$B = \frac{\mu_0 I R^2}{2(K^2 + X^2)^{3/2}}, \quad (1)$$

where B is the magnitude of the magnetic field, μ_0 is the permeability of air, I is current, K is the coil radius, and X is the distance between the point and the coil center. Hence, (1) implies that stronger magnetic fields were expected near the winding as the coil gets larger.

In the combined system, multi-coil structure determines the mutuality of transmitter coils, magnetizing inductances, efficiency, conduction, and switching losses. A special arrangement of coil inductance of transmitters as well as their interaction affects quality factor (Q). The quality factor in its most general simple form is given by,

$$Q = \frac{\omega L}{R}, \quad (2)$$

where ω is the operating frequency in terms of radians per second, L is the inductance of transmitter coil and R is the effective series resistance value. Equation (2) implies that $A4WP$ transmitter coil may not need as high of inductance to reach high-quality factor numbers because of already high frequency of operation. In contrast, Q_i transmitter coil must have higher inductance and hence it needs a larger area. In order to decrease the losses in the system, series coil resistance R value must decrease and one of the ways to achieve this is using *LITZ* wire. *LITZ* wire is a simple combination of thinner interwoven wire threads that prevents skin effects, especially, for 6.78-MHz operation. However, for the required turn ratios, it would occupy a larger volume than single wire coil and proximity effects would be more dominant for 6.78-MHz operation. While this option was more appropriate for the transmitter coils, low power and low charging pad area requirement of wearable devices made single-core Polyurethane Enamel Wire (*UEW*) option more attractive solution on the receiver side for such space limited case. Initial transmitter spiral coil approximate inductances in the air are calculated from Wheeler formula for flat coils which is approximated by;

$$L = \frac{N^2 K^2}{8K + 11w}, \quad (3)$$

$$K = \frac{D_i + N(w + s)}{2}, \quad (4)$$

where N is number of turns in the coil, K is related to physical coil dimensions and derived from (4), D_i is the inner diameter of the coil in mm, w is the wire diameter in mm, and s is the distance between windings in mm. According to (3) and (4), increasing the number of turns and inner diameter are the most effective ways to get larger inductances. The structure with the corresponding ferrite substrate thickness is also simulated in EM tool ADS as shown in Fig. 1. The effective Q_i inductance value variation with frequency, while having concentric $A4WP$ coil in the center is also shown in the same figure.

After the construction and concentric placement, an impedance meter measurement is conducted to obtain exact numbers

to determine the fine-tuning high-voltage capacitance amount needed for the series T_X resonance.

The final $A4WP$ transmitter coil of this design has 10 turns, 12 mm inner radius, and 19 mm outer radius. The inductance of this particular coil is 4.7 μH . Larger Q_i transmitter coil on the other hand has 20 turns, 26 mm inner radius, and 40 mm outer radius. The inductance of this outer coil is designed to be around 40 μH . The wires used in both transmitter coils had the same diameter of 0.6 mm. Various coil structures can be designed according to the target system specification. In this design, charging of rather small size devices is targeted, so the transmitter pad could not be as large in area, too. In order to improve the transfer efficiency, a ferrite sheet is placed underneath the transmitter coils. After insertion of the ferrite layers, the final measured inductance values for both coils were reported to be 7.65 μH for $A4WP$ coil and 71.2 μH for Q_i coil. The large discrepancy between the measured inductance values and the Electromagnetics (EM) simulated values was attributed to the ideal ferrite material permeability assumptions in simulations not matching to that of the real magnet used during the experiments. These final measured inductance values were considered while tuning the driver circuit capacitances for resonance. The small receiver coil on the other hand has 30 turns with a total outer diameter of 15 mm and wiring width of 1 mm. The single-lane thickness of the coil is very small and the coil has multilayer structure winding to reach a large inner diameter. By utilizing a wire whose diameter is 35-AWG (American wire gauge) (~ 0.15 mm), a small form factor receiver could be obtained. Thanks to large turn ratio, the total inductance value was measured to be 19.5 μH in this R_X coil. Although the resultant series R_X coil impedance was significantly higher in the order of multiple Ohms, it is not the limiting factor since the total power to be transferred was rather limited by the coil size. The R_X circuit is just a simple parallel resonance tuned only for high-frequency mode by slightly changing the coil inductance to match the parasitic diode device capacitance, which did not impact the reception of the low-frequency signal at large. Following the resonant tank is low-parasitic Schottky Diode full-wave rectifier that drives 100 Ω load experimental load along with a 1- μF smoothing capacitor.

Combo driver circuit structure

The block diagram for the output stage of the proposed main combo wireless power transfer system is shown in Fig. 2. The system involves two drivers working at the order of magnitude different frequencies driving two independent co-centric coils simultaneously in series resonance. Although the overall combo system was to be supplied from the same standard 5-V *USB* adapter, two individual driver circuits of both systems were also implemented separately with the possibility to optimize each of them independently. This is done as such to be able to compare performances of all three cases; Q_i only, $A4WP$ only and combo system; each optimized independently for maximum power transfer to the same exact target receiver load. $A4WP$ subsystem was optimized to be working at 6.78 MHz and the other one is at the higher end of Q_i standard at around 200 kHz. The receiver in the system designed as a wideband receive coil without any resonance capacitor to be able to receive both frequency signals and feed them into 0.25-V single Schottky rectifier followed by the load. Combining signals before rectification has two-fold benefits; first, it reduces the loss associated due to diode drop. Second and more important, it is rather an addition of the two signals directly

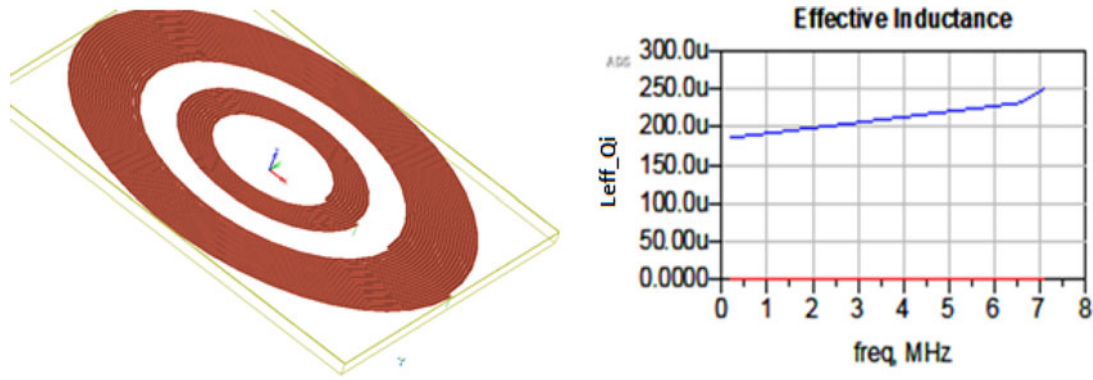


Fig. 1. The 3D EM modeling of the proposed concentric dual-band inductors.

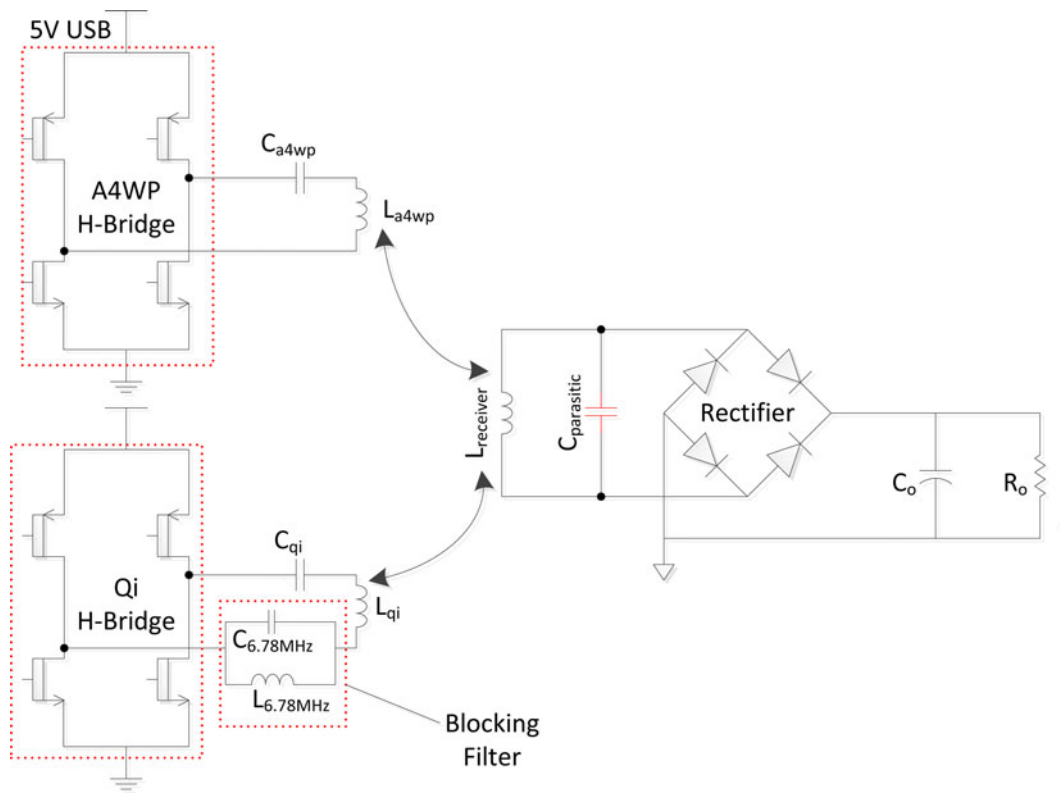


Fig. 2. Combined wireless power transfer system block diagram with blocking filter.

rather than an excess of rectifier drop type of combining. There were two main issues to be resolved in this particular combo scheme.

First, the loss associated is due to mutual loading of each T_X coils since they are placed one inside the other. The loading on the Q_i system due to high-frequency $A4WP$ system was left quite limited by choosing the 6.78-MHz coil inductance practically highest possible and hence the series resonance capacitor is minimal. In addition to reducing the loading effect on the Q_i transmitter, this would help the self-quality factor of the original high-frequency mode. In order to prevent the reverse leak of power from the 6.78-MHz coil back into the 200-KHz Q_i transmitter as a loss, the proposed system implements a blocking parallel resonance through $L_{6.78}$ and $C_{6.78\text{ MHz}}$. In this case, the parallel resonance blocking inductance was chosen minimum

possible with respect to the coil inductance of the Q_i system to minimize the loss in that side due to impedance division.

The second issue in this particular combo system is that the resonance can now be altered by not only the load variation but also, with the physical variation and placement of the accompanying sister driver system. However, automatic independent feedback loops around each of these two systems assure continuous resonance at each path regardless of any process, load, temperature, component or placement variations. The resonance control loop proposed for low-speed Q_i sub-system is quite different than the resonance control loop for $A4WP$ sub-system; both of which were separately studied and experimented with.

The schematic diagram of the Q_i control loop is shown in Fig. 3. There is no clock source in this circuit; the series resonance of the driver load is included as a part of feedback oscillator

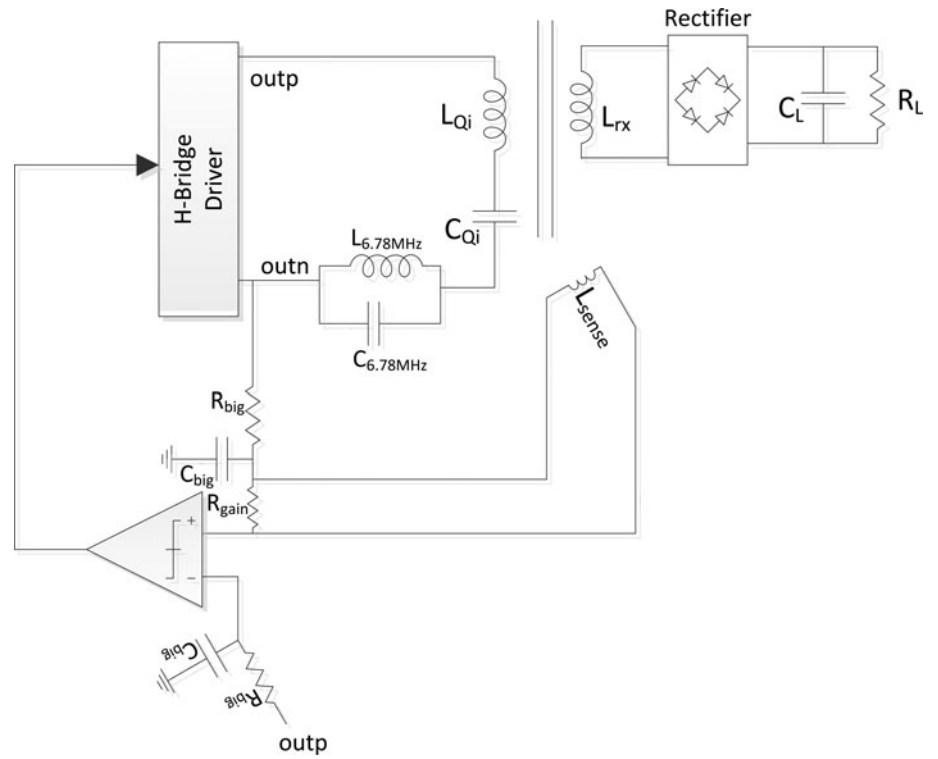


Fig. 3. Q_i sub-system analog automatic-tracking resonance lock loop.

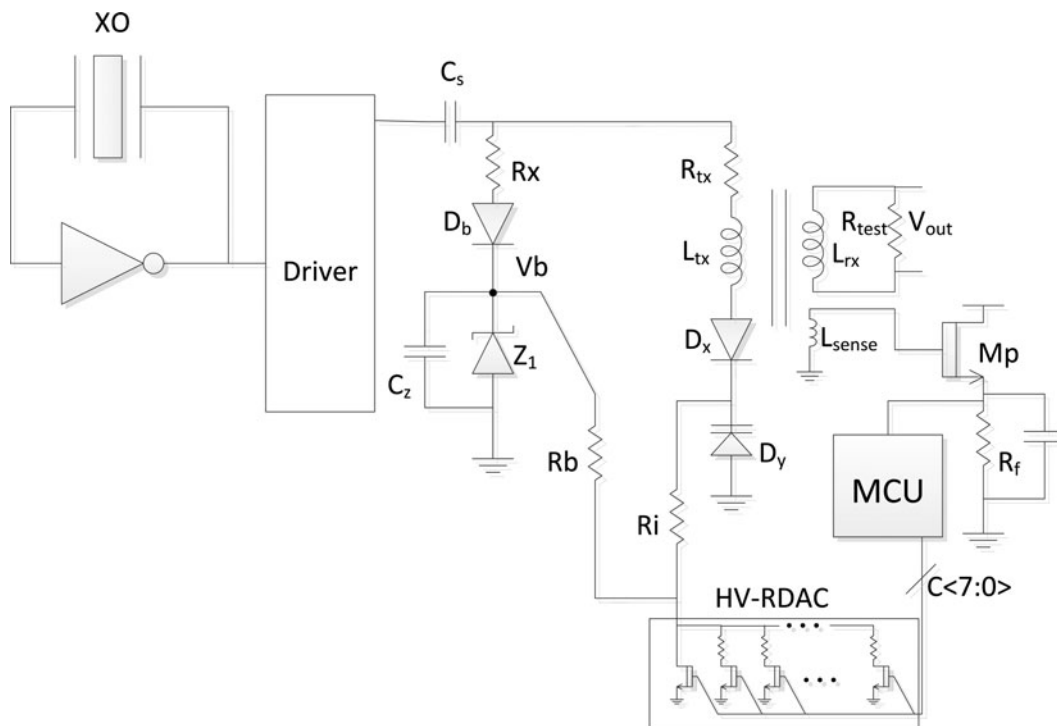


Fig. 4. High-speed $A4WP$ sub-system resonance lock loop.

utilizing a single fast high-gain comparator in the feedback. Feedback sense path is a wideband low gain inductive sensor with very low resistive gain (R_{gain}) which yields enough loop gain only at the resonance frequency and hence force the loop into peak gain resonance oscillation point. This analog feedback

loop adjusts itself automatically tracking any load or environmental changes continuously. The only drawback is that the frequency of the operation is not set precisely and depends on many of the factors mentioned above. However, this does not pose a serious problem for the Q_i standard which has a rather large operating

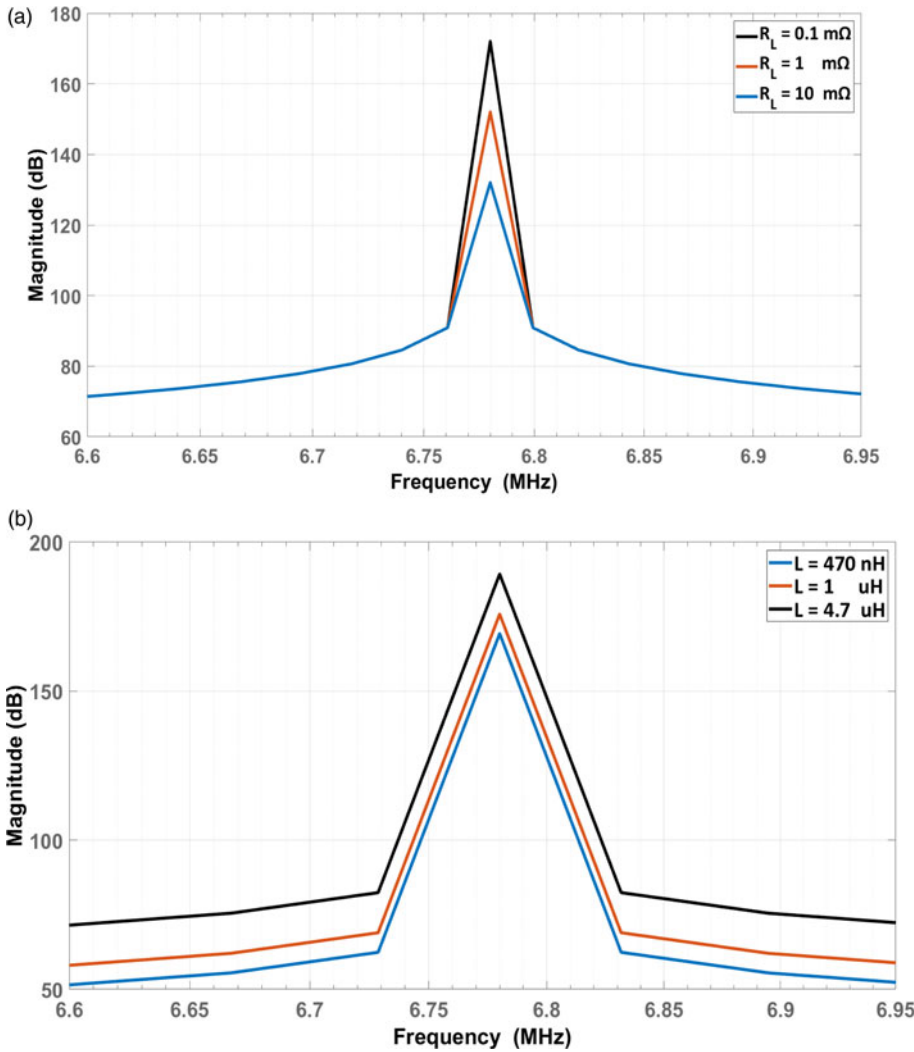


Fig. 5. (a) The bode diagram of Q factor of parallel LC filter by varying internal resistance of the inductor. (b) The bode diagram of Q factor of parallel LC filter by varying inductance value and capacitance value according to the resonance condition at 6.78 MHz.

frequency range, unlike *A4WP* standard frequency allocation. In this feedback loop, the DC common mode of the comparator is set by heavy filtering of both positive and negative outputs not to leave a chance for any stable latch-up lock condition without oscillation (in regular mode of high-frequency oscillation condition, both common modes ideally sit around mid-supply).

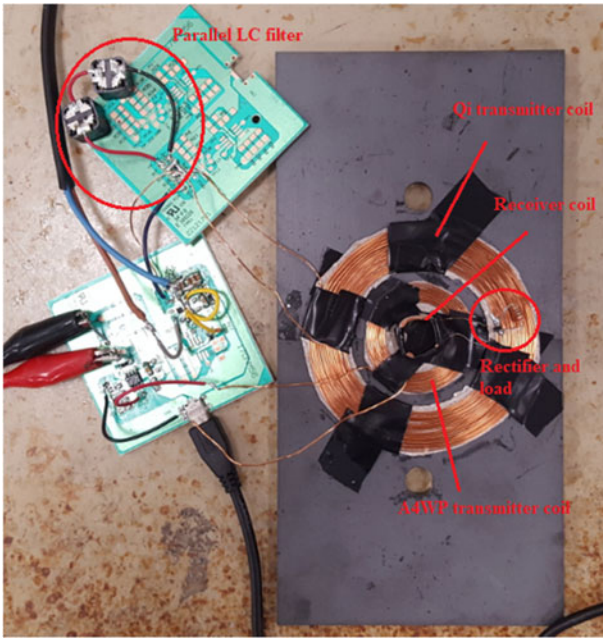
Schematic diagram of the high-frequency loop is shown in Fig. 4. Due to high-speed operation associated, an analog loop self-oscillation method proposed above cannot catch up with using low-cost active components. It is implemented using the digital feedback lock mechanism proposed in [11]. A 6.78-MHz Pierce crystal oscillator is employed as a signal source in this case due to stringent frequency accuracy requirement. The simplicity, low-cost nature, and frequency stability made such a design an attractive choice.

A simple inverter buffer sharpens the waveform into a switching power driver stage directly which is shown to be single-ended conceptually for simplicity. This buffer and the network in the actual implementation and measurements were rather fully differential H-bridge drivers, directly driving it in resonance through a waveform generator. The whole 6.78-MHz system operates from the same 5-V *USB* supply. The load for the driver is a series resonance formed by the primary charging coil L_{Tx} , a fixed series capacitor C_s and a series of back-to-back diodes that are used

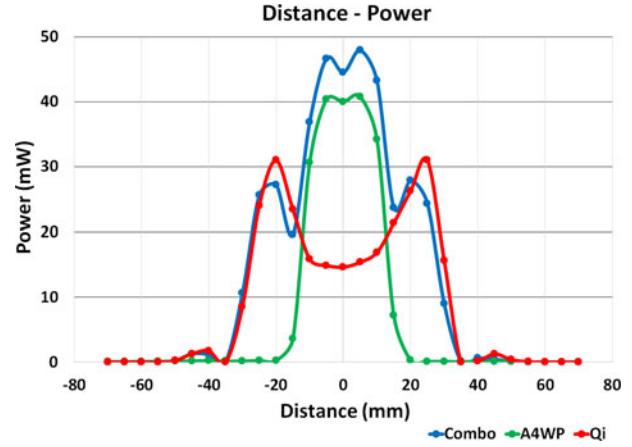
as tuning elements. The receiving side, which is a parallel resonance in the final design at 6.78 MHz, is just a fixed 470 Ω resistor for the time being to be able to characterize the frequency response of the transmitter independently. It should be noted that this design procedure holds true since the secondary R_x coil is extremely small relative to the T_x coil and hence may not load it significantly different when replaced by the resonance capacitor and the following rectifier. The tuning of the tank is done through high voltage DAC feedback. The current in the primary coil is sensed through another almost no cost printed circuit board (PCB) trace coil and the signal drives a peak detector directly. A source follower N-type Metal-Oxide-Semiconductor (NMOS) device with a large resistor and a large capacitor is used as a peak detector to retain the peak of the sensed signal from the primary driver coil. The peak detector output is digitized by a low-cost low pin-count microcontroller that implements peak search algorithm in order to continuously keep the loop around the maximum signal level which corresponds to resonance. The gain of the sense path is adjusted through the size and number of turns of this particular sense coil which is built as a spiral PCB inductor to fit into the dynamic range of the microcontroller Analog to Digital Converter (ADC). In order to maximize the tuning range with a given varactor diodes D_x and D_y , instead of using limited 5 V that was available as the

Table 1. Optimized component values for the proposed combo system

Symbol	Parameter values
C_{a4wp}	76 pF
L_{a4wp}	7.6 μ H
C_{qi}	7 nF
L_{qi}	68 μ H
$\hat{C}_{6.78 \text{ MHz}}$	95 pF
$L_{6.78 \text{ MHz}}$	4.7 μ H
$ESR_{L6.78 \text{ MHz}}$	3 mOhm

**Fig. 6.** Experimental prototype of the proposed combo system on a ferrite shield.

microcontroller supply, the design steals some tiny amount of current from the large resonance tank swing and generates up to 20 V reverse bias voltage to the diodes through a high voltage resistive control DAC. This is particularly important since the system itself as a power management circuit cannot expect to employ another power subsystem to generate the needed boosted supply level. It should be noted that in order not to impact the tank at these tap points, the first element used was a large value insulation resistor (R_x). The bias voltage is regulated with a simple low-cost Zener diode. If the 8-bit sense code from the microcontroller is all zeros then the control voltage is maximum defined by this Zener diode Z_1 . If on the other hand, all ones, then the last NMOS device in the chain assure that the tuning voltage can go down all the way close to zero by pulling down all the binary-weighted resistor string along the low-voltage controlled analog Digital-to-Analog Converter (DAC). Hence, a self-contained high voltage biasing scheme assures a maximum range with minimal quality factor degradation due to loss of resonance. Similarly, in order not to add any extra parasitic capacitance at the tuning node, another insulation resistor R_i is utilized. The value of this resistor is not critical and it should be placed right at the tuning point to avoid even the PCB routing capacitances to the tank.

**Fig. 7.** The measured total R_x power with respect to the position of receiver coil for all three types of transmitters.

Optimization of parallel LC filter

After Q_i transmitter and $A4WP$ transmitter are optimized individually, the output stages were combined together driving each at resonance with the proposed parallel resonance blocking filter. This filter is needed to prevent power loss due to the leakage inductance between transmitter coils. The way of blocking the 6.78-MHz signal wave on the 200-kHz circuit is to add a low-loss parallel resonance LC filter in series. When parallel LC combination resonates at 6.78 MHz, it theoretically poses high impedance to any coupling at 6.78 MHz. In fact, the internal resistances of components decrease the quality factor of the filter and the overall impedance of this parallel tank is lowered. Hence, quite low-effective series resistance (ESR) filter components were needed to get the best out of the proposed blocking technique with a higher Q -factor. The higher the Q -factor, the lesser is the damping and the rejection becomes more effective without undesired losses caused by this enhancement filter itself. According to equation (2), higher inductance ensured better filtering due to high Q . On the other hand, the inductance value of the non-radiative filter must be very low to prevent power loss on Q_i driver circuit. This discrete filter inductor behaves as a voltage divider and causes a drop in the peak voltage level reaching the main radiation coil. Graph of the Q factor values with effective coil impedance is shown in Fig. 5(a).

The filter was tuned manually first time around to fit it best at the target center frequency to minimize the loss of $A4WP$ transmitter leakage into Q_i network. After the parallel LC filter components were tuned, the Q_i transmitter has to be compensated for resonance once more because of the change in the impedance of the filter. The final component values and other parameters after iterative tuning and optimizations in the circuit are provided in Table 1. L_{a4wp} and L_{qi} coil inductance values are the final values after addition of a ferrite shield the test prototype system. The system-level design start strategy in determining the initial coil inductance values was to maximize the inductances while keeping a decent amount of capacitance not to leave the resonances sensitive to the tuning-knob and other PCB level parasitics on the PCB. High-frequency system had another constraint; self-resonance, which was the main limitation in the coil size and number of turns. Large inductance with a larger number of turns would yield more filed density if the source is current

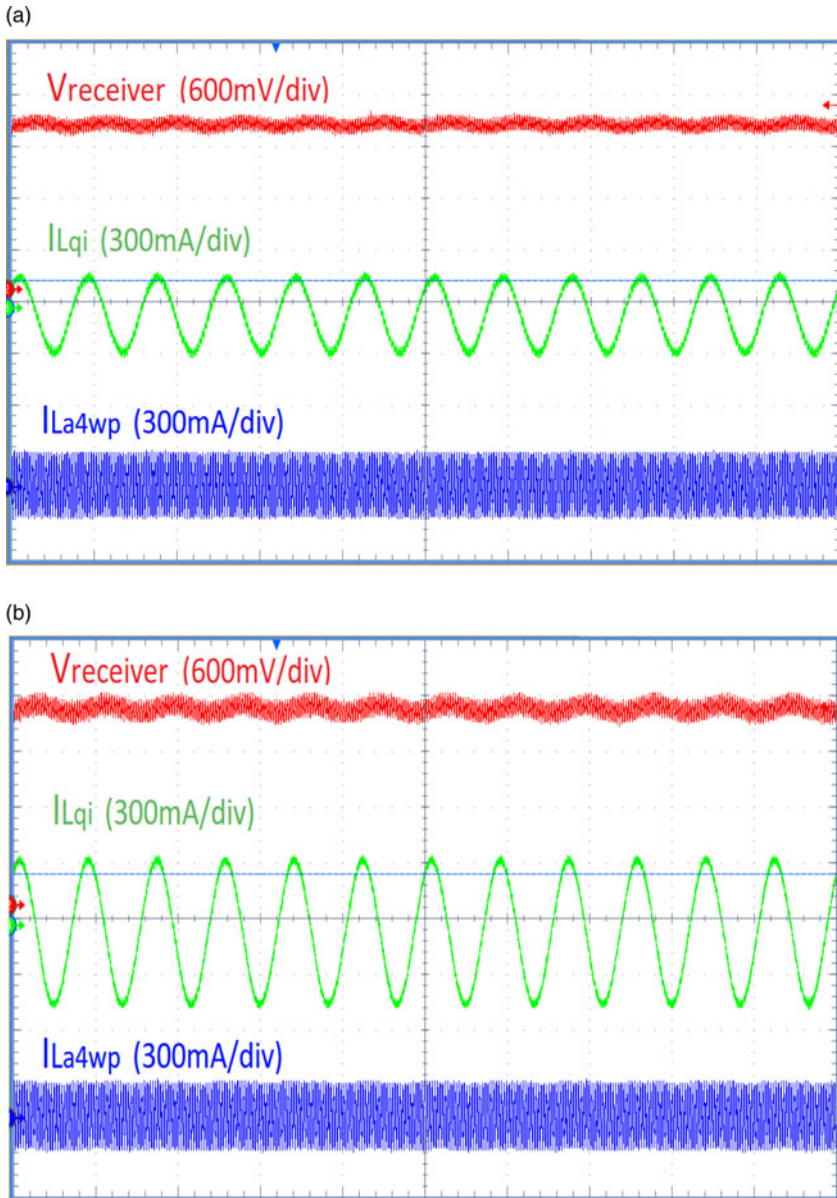


Fig. 8. (a) The measured output voltage and transmitter coil currents without parallel LC resonant filter. (b) With the blocking resonant filter in place.

limited (in the proposed system source is USB travel charger with 1-A and 5-V output and hence the main strategy was to maximize the inductances).

As depicted in equation (5), the overall target of the network in this Q_i driver path was to pose a low impedance for the switching power transistors at 200-KHz Q_i operation frequency, while at the same time blocking the 6.78 MHz coupling from the concentric A4WP coil. Equation (5) below defines the target load characteristic for the Q_i series transmitter impedance network which is first time tuned to the center frequency experimentally including all the parasitic elements on the PCB. After production, any external variations, such as component variations and exact physical location of the load are expected to be compensated by the proposed live feedback tuning mechanism.

$$Z_L + Z_C + \frac{Z_{L_{6.78\text{MHz}}} \times Z_{C_{6.78\text{MHz}}}}{Z_{L_{6.78\text{MHz}}} + Z_{C_{6.78\text{MHz}}}} = 0. \tag{5}$$

Experimental results

The proposed combo wireless charging system with 6.78 MHz parallel resonance blocking filter has been implemented and characterized in measurements. Figure 6 shows the picture of the initial experimental prototype of the proposed combo system on a ferrite shield.

In the experimental study, the receiver coil is moved from -70 mm to $+70$ mm over the centered transmitter coils along the X-axis coordinates and the total transferred power was measured at a constant resistive load R_O of 100Ω . This measurement is repeated separately for all three systems; namely, the mentioned combo system, A4WP only system, and Q_i only system in order to obtain spatial power transfer map for each design. A waveform generator is used to tune each of the sub-systems independently to their best resonance point with the load, in order to reach an apple-to-apple best obtainable performance comparison for all three cases. The resulting spatial power graph chart is shown in Fig. 7. It may be observed in this measurement figure that the

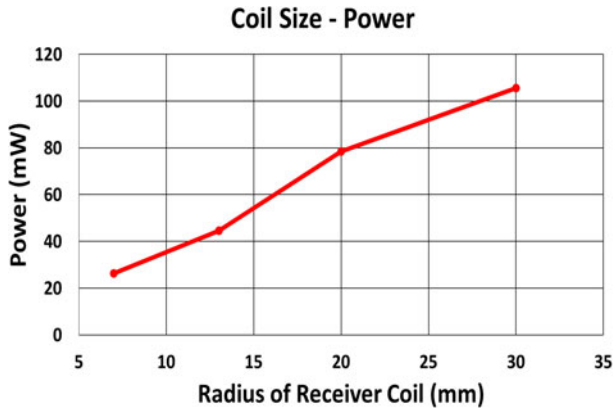


Fig. 9. Measurement results for output power versus 30-turn fixed coil radius.

proposed combo system could achieve significantly higher power transfer than *A4WP* system alone and again more power than Q_i system alone around the central regions of the charging pad. A more attractive feature of the combo system is that this particular level of received signal is well maintained across a wider range than each individual system alone. It effectively combined the best characteristics of the two distinct sub-systems thanks to the simultaneous operation, which provided stable R_x power levels across the mentioned large charging pad scan area. It should be emphasized that in order to reach a fair comparison, the 5 V source for all three designs was kept the same to be a realistic 5 V-1A *USB* travel charger unit. Each system was supplied from this limited source and each was independently optimized to provide the highest possible power transfer to an identically loaded receive coil.

Parallel LC resonant blocking filter effect is shown in Figs 8(a) and 8(b). The final rectified DC output voltage is measured as 1.907 V on the 100 Ω load and it corresponds to 36.36 mW power transfer in the system without parallel LC filter when tuned for maximum possible signal level.

Adding the resonant blocking filter and re-tuning the system increases the final rectified output voltage level to 2.113 V, increasing the total transferred power level to 44.64 mW. Adding the particular resonant filter reduced the power loss and increased the total amount of transferred power level approximately by 23%. Moreover, 6.78 MHz noise reduction in I_{Lqi} was visible from the difference in Figs 8(a) and 8(b) oscilloscope measurement plots; resulting in a better EMI performance as well.

Finally, in order to demonstrate the added value of more and spatially stable robust power distribution to small form factor wearable devices across the pad, the amount of power that could be transferred is plotted in Fig. 9 as a function of receiver coil size for the mentioned 30-turn Schottky rectified receiver design. It is quite clear that extracting the useful amount of power, for coil radiuses below 10 mm is a challenging task. Hence, any improvement in the amount of power that could be transferred to the device with a limited size is considered to be a value.

Conclusion

This work has introduced a dual-transmitter, single-receiver, combo wireless power transfer system for small size wearable devices. The comparative study of the current competing charging

Table 2. Performance comparison with respect to various other studies in the literature

Literature	Operating frequency	R_x coil size (mm)	Output power (mW)	Efficiency (%)
[22]	8.3 MHz	13	28.3	50
[23]	742 KHz	19	33	85
[24]	13.56 MHz	10	NA	73.46
[25]	13.56 MHz	10	NA	27.7
[26]	3.5 MHz	12.5	1.05	30.97
This work	230 KHz + 6.78 MHz	13	44.64	15

standards was also involved in measurements to be able to draw fair conclusions regarding the performance of the proposed system. It has been shown that the combo design with blocking resonant filter could provide not only more power in comparison to standard methods but also, yielded a more uniform power transfer profile with much wider spatial coverage without any snap or lock mechanism in place. A critical feature of the comparison technique is that the system was supplied from the same limited 5 V standard *USB* wall charger power source in a similar pad area arrangement, which also implied an apple-to-apple comparison. The work suggested that utilizing the simultaneous Q_i and *A4WP* transmission carefully with precision analog resonance loops could result in performance improvement. In addition to main combo charger idea, many circuit-level techniques such as low frequency oscillating auto-tuning loop as well as a high-speed digital feedback loop were all introduced as critical circuit building blocks of the proposed scheme. The low-frequency analog loop finds the exact resonance automatically for Q_i subsystem, while a digital detection loop changes a special varactor trim-cap around the loop to maintain auto-resonance.

The performance of the proposed system is also compared with the prior literature and the performance metrics belonging to these arts are presented in Table 2. The efficiency of the proposed system is relatively low due to the large transmitter pad area intended for user comfort. The target of this particular application is rather wide-area uniform power distribution; hence the efficiency was not a stringent design criterion.

Future work

Although the co-centric coils were carefully designed and optimized for the particular design, there can be more effort to improve the combo power transfer by exploiting rather two-dimensional coil designs. The current design did utilize only planar coils, which helps the transfer efficiency for the individual systems but hurt the combined one. There is a chance that by changing the center *A4WP* coil structure to rather multi-layered turns and hence leaving less metallization on the path of Q_i fields, power transfer efficiency could further be improved.

Acknowledgements. Authors would like to thank Dr. Ahmed Emira of Goodix Inc. for his valuable ideas in analog auto-tracking feedback loop design, NaveddUllah of Özyeğin University for his support in EM modeling and Vestel Power Electronics Research Labs for their valuable support during the test and characterizations as well as their support in custom coil construction efforts.

References

1. **Imura T and Hori Y** (2011) Maximizing air gap and efficiency of magnetic resonant coupling for wireless power transfer using equivalent circuit and Neumann formula. *IEEE Transactions on Industrial Electronics* **58**, 4746–4752.
2. **Berger A, Agostinelli M, Vesti S, Oliver JA, Cobos JA and Huemer M** (2015) Phase-shift and amplitude control for an active rectifier to maximize the efficiency and extracted power of a wireless power transfer system. Proceedings of IEEE-APEC, Charlotte, NC, USA, pp. 1620–1624.
3. **Cove SR, Ordonez M, Shafiei N and Zhu J** (2016) Improving wireless power transfer efficiency using hollow windings with track-width-ratio. *IEEE Transactions on Power Electronics* **31**, 6524–6533.
4. **Zhu Q, Su M, Sun Y, Tang W and Hu AP** (2018) Field orientation based on current amplitude and phase angle control for wireless power transfer. *IEEE Transactions on Industrial Electronics* **65**, 4758–4770.
5. **Zhang Y, Lu T, Zhao Z, He F, Chen K and Yuan L** (2015) Quasi-uniform magnetic field generated by multiple transmitters of magnetically-coupled resonant wireless power transfer. Proceedings of IEEE-ICEMS, Pattaya, Thailand, pp. 1030–1034.
6. **You Y, Soong BH, Ramachandran S and Liu W** (2010) Palm size charging platform with uniform wireless power transfer. Proceedings of IEEE International Conference on Control Automation, Robotics & Vision, Singapore, Singapore, pp. 85–89.
7. **Casanova JJ, Low ZN, Lin J and Tseng R** (2009) Transmitting coil achieving uniform magnetic field distribution for planar wireless power transfer system. Proceedings of IEEE Radio and Wireless Symposium, San Diego, CA, USA, pp. 530–533.
8. **Wireless Power Consortium** (2017) The qi Wireless Power transfer system power class 0 specification, v1.2.3, Parts 1 and 2: interface definitions.
9. **Galizzi M, Caldara M, Re V and Vitali A** (2013) A novel qi-standard compliant full-bridge wireless power charger for low power devices. Proceedings of IEEE WPT, Perugia, Italy, pp. 44–47.
10. **Waffenschmidt E** (2011) Wireless power for mobile devices. Proceedings of IEEE INTELEC, Amsterdam, Netherlands, pp. 1–9.
11. **Abouzeid MO and Tekin A** (2017) Adaptive 6.78-MHz ISM band wireless charging for small form factor receivers. Proceedings of IEEE ISCAS, Baltimore, MD, USA, pp. 1–4.
12. **Park Y-J, Jang B, Park S-M, Ryu H-C, Oh SJ, Kim S-Y, Pu Y, Yoo S-S, Hwang KC, Yang Y, Lee M and Lee K-Y** (2018) A triple-mode wireless power-receiving unit with 85.5% system efficiency for a4wp, wpc, and pma applications. *IEEE Transactions on Power Electronics* **33**, 3141–3156.
13. **Johns B, Antonacci T and Siddabattula K** (2012) Designing a qi-compliant receiver coil for wireless power systems, part1, TI. [Online] Available at <https://www.mouser.com/pdfDocs/TI-Designing-a-Qi-compliant-receiver-coil.pdf>.
14. **Chen MX and Cheng KWE** (2017) Design of flat magnetic core for inductively coupled coils in high efficiency wireless power transfer application. Proceedings of International Conference PESA-Smart Mobility, Power Transfer & Security, Hong Kong, China, pp. 1–7.
15. **Campi T and Feliziani SCM** (2014) Magnetic shielding of wireless power transfer systems. Proceedings of International Symposium EMC, Tokyo, Japan, pp. 422–425.
16. **Ahn D, Kim S, Kim S-W, Moon J and Cho I** (2017) Wireless power transmitter and receiver supporting 200-kHz and 6.78-MHz dual-band operation without magnetic field canceling. *IEEE Transactions on Power Electronics* **32**, 7068–7082.
17. **Zhao C and Costinett D** (2017) Gan based dual-mode wireless power transfer using multifrequency programmed pulse width modulation. *IEEE Transactions on Industrial Electronics* **64**, 9165–9176.
18. **Riehl PS, Satyamoorthy A, Akram H, Yen Y-C, Yang J-C, Juan B, Lee C-M, Lin F-C, Muratov V, Plumb W and Tustin PF** (2015) Wireless power systems for mobile devices supporting inductive and resonant operating modes. *IEEE Transactions on Microwave Theory and Techniques* **63**, 780–790.
19. **Rooij M and Zhang Y** (2016) A 10 W multi-mode capable wireless power amplifier for mobile devices. Proceedings of IEEE PCIM, Shanghai, China, pp. 1–8.
20. **Burket C** (2017) Wireless charging opportunities and challenges for wearables: one size does not fit all. *IEEE Power Electronics Magazine* **4**, 53–57.
21. **Roshan YM and Park EJ** (2017) Design approach for a wireless power transfer system for wristband wearable devices. *IET Power Electronics* **10**, 931–937.
22. **Cannon BL, Hoburg JF, Stancil DD and Goldstein SC** (2009) Magnetic resonant coupling as a potential means for wireless power transfer to multiple small receivers. *IEEE Transactions on Power Electronics* **24**, 1819–1825.
23. **Li X, Zhang H, Peng F, Li Y, Yang T, Wang B and Fang D** (2012) A wireless magnetic resonance energy transfer system for microimplantable medical sensors. *Sensors* **12**, 10292–10308.
24. **Ezzulddin AS and Ibraheem AA** (2017) Design and optimization of printed spiral coils used in wireless power transmission systems for powering 10 mm² receiver size at 13.56 MHz operating frequency. *International Journal of Current Engineering and Technology* **7**, 1835–1841.
25. **Jow U and Ghovanloo M** (2009) Modeling and optimization of printed spiral coils in air, saline, and muscle tissue environments. *IEEE transactions on Biomedical Circuits and Systems* **3**, 339–347.
26. **Ko WH, Liang SP and Fung CDF** (1977) Design of radio frequency coils for implant instruments. *Medical & Biological Engineering & Computing Journal*, 634–640.



Üstün Sağlam received the B.S. degree in electrical and electronics engineering from Hacettepe University, Ankara, Turkey in 2015. Since 2016, he has been the candidate of M.Sc. degree in electrical and electronics engineering at Özyeğin University. He is a senior design engineer at Power Electronics Research Center, Vestel Electronics, Manisa, Turkey. His research interests include the design and the development of switching mode power supplies and wireless power transfer systems.



Ahmet Tekin has received his EE Ph.D. degree from University of California Santa Cruz, CA, EE MS degree from North Carolina A&T State University, Greensboro, NC and EE BS degree from Bogazici University, Istanbul, Turkey in 2008, 2004, and 2002, respectively. In addition to academic research in microelectronics, he worked for multiple innovative semiconductor design companies such as; Multigig, Inc., Newport Media, Aydeekay LLC, Broadcom corp., Semtech Corp., Nuvoton Technology Corp., Qualcomm and Waveworks Inc., leading designs for communications, consumer and medical markets. His main focus area is analog/RF/mixed-signal integrated circuit design for communication and biomedical applications. He is currently director of Analog&RF Labs at Özyeğin University and serves as a member of board of directors at Waveworks Inc, Mission Viejo, CA.